

## **Teilprojekt B2.10**

### **Time-Dependent Electron Transport Through Nanostructures**

**Projektleiter:** Ferdinand Evers, Peter Schmitteckert, Peter Wölfle

**CFN-Financed Scientists:** Dr. Dmitry Aristov (E13, 11 months), Alexander Branschädel (E13/2, 8 months), Dr. Marion Moliner (E13, 12 months), Dr. Verena Koerting (E13/4, 9 months), Dr. Holger Schmidt (E13, 2 months)

**Further Scientists:** Dr. Tobias Ulbricht/Küchel (TKM), Prof. Hubert Saleur (Paris), Prof. Edouard Boulat (Paris), Dr. Max Köntopp (Rutgers U, USA), Dr. Dan Bohr (Copenhagen), Dr. Alexei Bagrets (INT), Dr. V. Meded (INT), Prof. Kieron Burke (Irvine), Dr. Martin Greiter (TKM), Prof. Xin Wan (Hangzhou U, China), Prof. Rafael Molina (Madrid),

**Institut für Theorie der Kondensierten Materie (TKM)  
Karlsruhe Institute of Technology**

**Institute of Nanotechnology (INT)  
Karlsruhe Institute of Technology**

## Time-Dependent Electron Transport Through Nanostructures

### Summary

The aim of this project is the description of the transport of electric charge or spin through point contacts, quantum dots or quantum wires in the presence of strong correlations. Here we developed numerical approaches based on the density matrix renormalization group technique (DMRG) and an analytical approach to junctions of Luttinger liquid wires. First we implemented the Kubo response function to determine the linear conductance in the presence of strong correlations. Using real-time simulations within time-dependent DMRG (td-DMRG) we obtained the finite bias I/V curve and noise correlations for the interacting resonant level model and found excellent agreement with analytical calculations based on the thermodynamic Bethe ansatz. Recently we obtained the I/V curve of the Kondo model in the strong coupling regime. In addition we studied spin charge separation in a transport experiment. Finally we extracted exact Kohn-Sham density functional theory (DFT) potentials and compared the linear response DMRG results with linear response calculations within the DFT Kohn-Sham auxiliary system.

Following the success of the td-DMRG we are currently simulating the Full Counting Statistics (FCS) based on real-time simulations of the cumulant generating function (CGF). We are extending the td-DMRG to handle driven system and are testing reflectionless impurities to increase the resolution of transport simulations. As a new approach to access nonequilibrium states we developed an adiabatic evolution of states.

In cooperation with Kurt Busch (A1) we have simulated light matter interaction at a two level systems embedded into onedimensional waveguiding structures.

In addition to the above numerical studies, we have developed an analytical method to calculate the conductance matrix of a junction of quantum wires modelled as Luttinger liquids.

### 1. Spin charge separation

The spin charge separation of a single electron excitation is a prominent example of interaction effects in one-dimensional electron systems. The first numerical observation was performed with an exact diagonalization approach by Hallberg et al. [1] for a 16 site system. Kollath et al. [2] reported a simulation on a 72 site system with hard wall boundary conditions and 56 electrons. In [B2.10:6] we showed that with our code it is possible to study spin charge separation within the framework of time-dependent DMRG (td-DMRG) for a 1/3 filled 33 site Hubbard chain with periodic boundary conditions (PBC) keeping up to 10000 states per DMRG block. It turned out that for accurate results we should at least use the order of 2000 states per block, which is considerably more than applied in [B2.10:7]. We compared [B2.10:7] the results of Kollath et al. [2] (KSZ) who employed an adaptive td-DMRG scheme combined with a Trotter decomposition [3,4] with results obtained from our code where we combined the adaptive scheme with a Krylov based matrix exponential [5]. The system is a 72 site Hubbard model with an on-site interaction of  $U=4.0$ . The perturbation was created by applying a Gaussian perturbation to the potential of the up-electrons in the same way as described in [5]. By taking up to 5000 states per block we have been able to demonstrate that the results obtained by KSZ had an error of more than 100% in the spin sector.

Having established our code we asked the question whether one should be able to observe the spin charge separation in a transport setup [B2.10:12]. We have therefore attached an interacting region to non-interacting leads. We then created a single, left moving hole excitation in the right lead and let it evolve. At the end of this scattering process of a single electronic excitation, one may ask what we end up with. The main question that arises is,

whether the outcome will be well defined spin-charge separated wave packets, or if a hole will be reconstructed, since we took out one electron of the system in the beginning, or if there will emerge an incoherent superposition of many excitations.

The transport setup displayed in Figure 1 consists of 100 sites, divided into 41 left lead sites, 29 interacting sites and 30 right lead sites. Upon the ground state we created a single hole

$$\frac{1}{N} \sum_k e^{-\frac{(k-k_0)^2}{2\sigma^2}} c_k |\Psi_0\rangle$$

excitation in the right lead using a Gaussian distribution of annihilation operators with momenta  $k_0$ , of width  $\sigma$ , and  $N$  is the normalization to one.

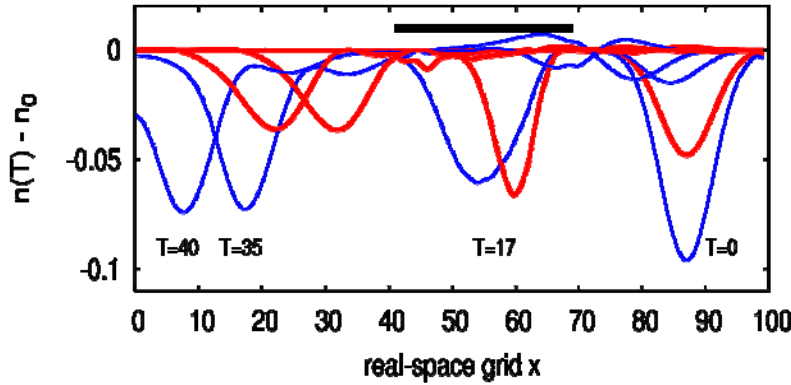


*Figure 1:* Spin charge separation in a transport experiment: Spin (thick, red) and charge (thin, blue) densities were subtracted from the background of the ground state system without an additional excitation. A hole created in the right lead ( $T=0$ ) passes the interacting nanostructure (black bar) undergoing SCS ( $T=17$ ). In the left lead spin and charge densities travel independently with equal velocity ( $T=35,40$ ).

With 48 down and 48 up electrons the non-interacting system was at half-filling and the interacting system with an onsite Hubbard interaction was kept at a filling of  $\sim 0.43$  and the injected hole had an average momentum of  $k_0 = 0.43\pi - 2\sigma$ , where  $\sigma = 0.03$ . This ensured the ability of the hole to tunnel into and out of the interacting region and keeping the transmission amplitude maximal. In Figure 1 we display the time evolution of the hole excitation for several time steps, where we have subtracted the background of the system without an excitation. Additionally, we averaged over Friedel oscillations. The data nicely shows that the wave packet undergoes a spin-charge separation and finally one ends up with a charge and a spin excitation travelling separately but with equal speed in the left lead. To this end, there is no reason for a recombination of spin and charge degrees of freedom to a single hole excitation. Nevertheless the outgoing wave packets are well defined and, in principle, the charge density and the spin density should be measurable in a time-resolved measurement of a spin-polarized charge density.

In order to identify spin and charge excitations we calculated the spectral function [B2.10:23] of a polarized Hubbard model and showed, that one can follow the charge and spin peaks while switching on a magnetic field. In the full polarized system the spin peak vanishes, which allows for an identification of the spin and charge peaks.

## 2. Linear response with momentum leads

Linear response calculations within DMRG [B2.10:2] provide a method to calculate the conductance of a nanostructure attached to leads. As it is based on the exact Kubo formula for the linear conductance it is valid for arbitrary interaction. In the DC limit the conductance can

$$g_{J_j N} = -\frac{e^2}{h} \langle \psi_0 | \hat{J}_{n_j} \frac{4\pi i \eta}{(\hat{H}_0 - E_0)^2 + \eta^2} \hat{N} | \psi_0 \rangle,$$

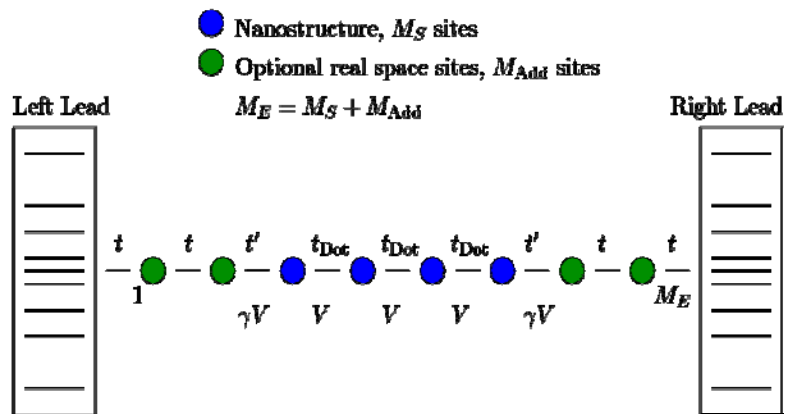
$$g_{JJ} = \frac{e^2}{h} \langle \psi_0 | \hat{J}_{n_1} \frac{8\pi \eta (\hat{H}_0 - E_0)}{[(\hat{H}_0 - E_0)^2 + \eta^2]^2} \hat{J}_{n_2} | \psi_0 \rangle,$$

be expressed in terms of two different correlators,

where the positions are in principle arbitrary. However, the positions should be placed close to the nanostructure to minimize finite size effects. In [B2.10:2] we introduced exponentially reduced hopping terms close to the boundary of the leads which had been described in real space to minimize finite size effects, which in return leads to ill-conditioned linear systems. In order to solve these equations, we had to employ scaling sweeps to switch on the damping in the leads gradually (see also sec. 7.3). While the method proved to be a valuable tool it turned out that it is getting too expensive to study more interesting systems.

To overcome these difficulties we developed a new scheme [B2.10:8] based on leads described in momentum space to overcome the difficulties we encountered in [B2.10:2], for details see also [B2.10:6,B2.10:25]. While it is generally accepted that DMRG does not work well in a momentum space description due to the large amount of couplings intersecting the artificial cut of the system into two parts within DMRG, our transport calculations are performed with non-interacting leads. Therefore the number of links intersecting the DMRG splitting of the system is vastly reduced.

*Figure 2:* Schematics of the leads coupled to the nanostructure. Blue dots indicate interacting region (on link interaction,  $V$ ), while green dots denote the piece of the leads explicitly kept in the iterative DMRG scheme. The coupling of the nanostructure to its environment is controlled by the hopping matrix element  $t' < t$ . The left and right boxes denote the reservoirs and the energy resolution of their states applied in our modelling.



In order to be able to describe processes on different energy scales we first couple our nanostructure to a few sites in real space to capture local, i.e. high energy, physics. Then we employ a logarithmic discretization of the momentum leads to cover a large energy range and finally we use a linear discretization of the low energy scale in order to describe low energy transport properties accurately. We would like to note that these additional sites on a linear discretization close to the Fermi edge are beyond a NRG like description. While they are not needed for a qualitative description, they enable us to get very accurate results even close to the resonant tunnelling regime. The reason for that lies in the nature of transport properties, where the  $\eta$  in the correlation function plays a much more important role than for equilibrium properties. It does not only provide a smoothing of the poles, it has to create excitations which then can actually lead to transport. For discretization details we refer to [B2.10:25].

Here we report on the result for the interacting resonant level model (IRLM) and the natural extension of this model to linear chains, defined by the Hamiltonians

$$\begin{aligned}
 H_{RS} &= \sum_{j \in S} \mu_g \hat{c}_j^\dagger \hat{c}_j - \sum_{j,j-1 \in S_E} (t_j \hat{c}_j^\dagger \hat{c}_{j-1} + \text{h.c.}) \\
 &\quad + \sum_{j,j-1 \in S_E} V_j \left( \hat{n}_j - \frac{1}{2} \right) \left( \hat{n}_{j-1} - \frac{1}{2} \right), \\
 H_{MS} &= \sum_{i \in L,R} \epsilon_i \hat{c}_i^\dagger \hat{c}_i, \\
 H_T &= -t \left( \sum_{i \in L} \hat{c}_i^\dagger \hat{c}_1 + \sum_{i \in R} \hat{c}_i^\dagger \hat{c}_{M_E} \right) + \text{h.c.},
 \end{aligned}$$

where  $c_\ell^\dagger$  and  $c_\ell$  ( $c_k$ ) are the spinless fermionic creation and annihilation operators at site  $\ell$  (momentum  $k$ ),  $H_{RS}$ ,  $H_{MS}$ , and  $H_T$  denote real space, momentum space, and tunneling between real- and momentum space Hamiltonians respectively. The symbols  $S$  and  $S_E$  denote the nanostructure and the extended nanostructure (the full real space chain), respectively. The indices  $L$  and  $M_E$  denote the first and last site in  $S_E$ . The general setup and the specific values of the hopping matrix elements and the interactions are indicated in Fig. 2, and denote specifically the interactions on the contact links,  $\gamma V$ . The momentum dependent coupling is chosen to represent an infinite one-dimensional tight-binding chain if a cosine band is chosen. All energies are measured in units of  $t=1$ .

In Figure 3 we show the linear conductance versus gate potential for a contact hopping of  $t'=0.01$  and interaction on the contacts ranging from  $V=0$  to 25. The calculations have been performed with 130 sites in total, real space sites, and 120 momentum space sites. Due to the symmetry of the band we used a discretization that is symmetric at the Fermi level, and applied an identical discretization scheme to both leads. To represent the ‘large’ energy span in the band we used 20 logarithmically scaled sites, and thereafter used 10 linearly spaced sites to represent the low energy scale correctly. In the DMRG calculations presented we used at least 1300 states per block and 10 finite lattice sweeps.

The data demonstrates a strong increase of the resonance width due to interaction up to a factor of ten. The increase of the resonance width due to interaction on the contact is in contrast to the reduction of conductance due to interaction on nanostructures, see [B2.10:8]. Once interaction is larger than the Fermi velocity the resonance width gets strongly reduced. The results also show that we can now resolve a resonance width of the order of 0.0001. We would like to note that this scheme is not restricted to single impurity models and that it also works for extended nanostructures as shown in [B2.10:8,B2.10:13]. We have applied this approach to the Single Impurity Anderson model with ferromagnetic leads [B2.10:19] and to the transport through ring structures.

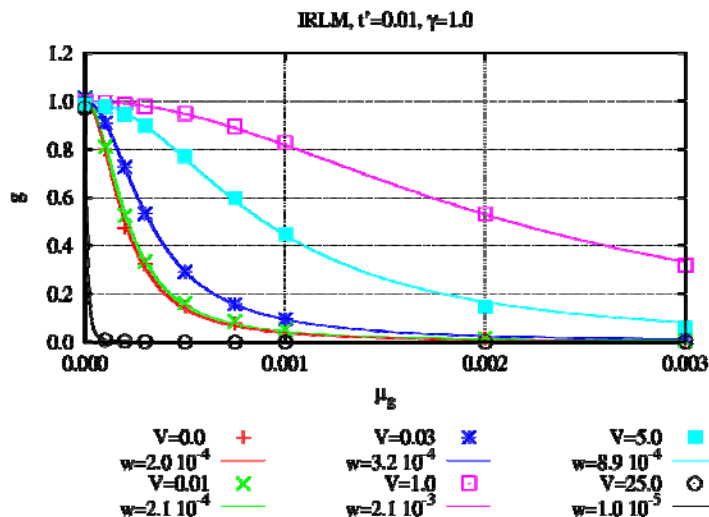


Figure 3: Linear conductance versus gate potential,  $\mu_g$ , for the interacting resonant level model for  $t'=0.01$  and a interaction,  $V$ , on the contacts ranging from zero to 25. To each set of DMRG data a Lorentzian of half width  $2w$  has been added as a guide to the eye. The leads are described with a cosine band such that the Fermi velocity is  $2t$ . In contrast to intradot interaction the interaction on the contacts enhances the conductance and shows a non monotonic behavior versus contact interaction.

### 3. Differential conductance and shot noise in the interacting resonant level model

The major problem in non-equilibrium dynamics consists in the fact that the stationary Schrödinger equation is replaced by the time-dependent Schrödinger equation. Therefore an *eigenvalue problem* is replaced by a *boundary problem* and one has to take care of the initial state. Therefore one has to be very careful by sending all difficult steps to time equal minus infinity since at some time one hits the initial state. In our approach the answer to this problem is to start with an initial state and to perform the full time integration of the time dependent Schrödinger equation via a time evolution operator given by the matrix exponential [5]. The method is described in [B2.10:6, 12] and reviewed in [B2.10:27].

In this project we concentrated on the interacting resonant level model. In this model a single level is attached to non-interacting leads via a hybridization amplitude  $t'$  and an interaction  $U$  on the contact links. Mehta und Andrei [6] claim to have solved the non-equilibrium transport problem via a scattering state Bethe ansatz. In our previous work using the Kubo approach within DMRG [B2.10:2,B2.10:8] we showed that repulsive interaction on the contact link leads to an increase of the resonance width of the linear conductance vs. gate voltage up to an interaction strength of the order of the Fermi velocity of the leads. Here we are looking at the finite bias conductance where the level is on resonance, i.e. we use a particle hole symmetric interaction without an additional gate voltage.

In pushing the calculations to the strong bias voltage regime we realized that one has to be careful with the initial state as one can get stuck with an excited state which leads to a voltage drop which is slightly smaller than the correct applied value. In addition we realized that the adaptive time evolution scheme is not reliable in the regime of strong bias voltages. Therefore we developed the following scheme. First we perform a ground state DMRG calculation without time evolution to find the correct initial state using up to 3000 states per DMRG block. We then perform a full time evolution using the matrix described within the framework of Krylov spaces [5]. We choose the time frame to be large enough to cover most of the transient regime. This step takes typically a week on a quad core node and up to three weeks for the 3000 states per block calculation on a 120 site system. Finally we continue with an

adaptive time evolution to cover a larger time frame within the quasi stationary regime.

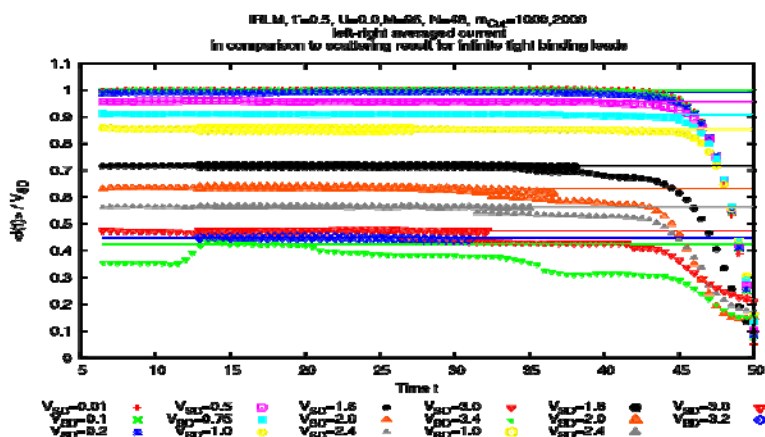


Figure 4: Current  $I(t)$  divided by the applied voltage,  $V_{SD}$ , vs. time for a set of applied source drain voltages. The smaller symbols correspond to 1000 states per block, the larger symbols to 2000 states per block. Results are from adaptive time sweeps after an initial full time DMRG up to  $t=5$ . The lines correspond to the exact result for infinite leads. The plot shows that for small voltages it is more than sufficient to use 1000 states per DMRG block. For large voltages one should use at least 2000 states per block to ensure a quantitative current measurement.

In Fig. 4 we plot the current  $I(t)$  divided by the applied voltage for a 96 site system with a non-interacting coupling using  $t'=0.5$ . Here we used a full time DMRG only up to  $t=5$ . The small symbols correspond to 1000 states per block, while the larger symbols correspond to 2000 states per block. The lines are given by the analytical result for the noninteracting system for infinite tight binding leads. The drop of the current around time  $t=48$  is related to

the back reflection of the wave packets at the end of the leads and corresponds to the transit time. For longer time scales we would have to use longer leads. The deviation of the current from a straight line after the settling time is related to truncation errors of the adaptive time evolution scheme. The sharp drops in this regime are related to a missing renormalization of the wave function at the restart of the adaptive time evolution scheme. Actually, due to unitarity of the time evolution operator the time dependent wave function should always be normalized. However, due to the projective nature of the adaptive time evolution scheme one loses weight at each DMRG step.

While the results are fine in the not too strong voltage regime they also show that one has to be very careful in the large voltage regime. Since we are especially interested in the latter regime we employed the approach described above and double checked our results by taking up to 3000 states per block. Finally we increased the full time DMRG regime to  $T=10$ . By carefully fitting the current left and right the impurity vs. time  $T$  and checking for the oscillations, compare [B2.10:6,B2.10:27], in the quasi stationary regime we obtain the results displayed in Figure 5 for a hybridization of  $t'=0.5$  [B2.10:11]. The red line shows the analytical result including the energy dependent transmission due to the cosine band. The red plusses (crosses) are obtained by fitting the current left (right) of the impurity. The results show that calculations using 2000 states per block reproduce the analytical result even in the large bias regime. Note that the units are given by the hopping elements of the tight binding leads leading to a band width of  $4t$ . The results are done for  $M=96$  sites and 48 fermions using

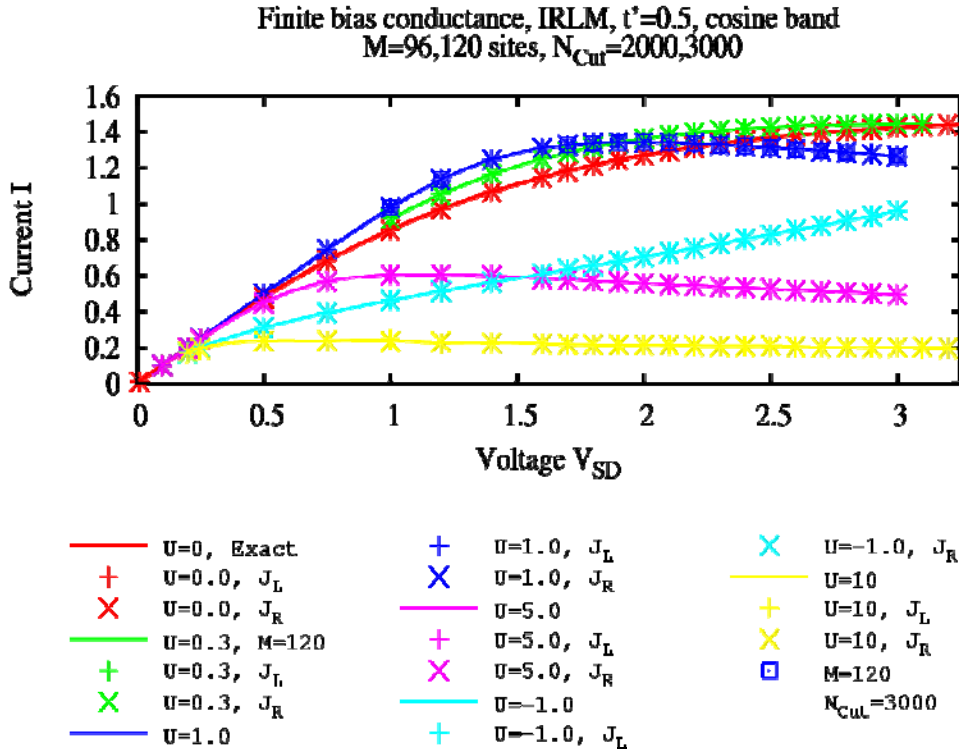


Figure 5: I/V curve for the interacting resonant level model for different values of the on-link interaction  $U$ , and system sizes  $M$ .  $J_L$  ( $J_R$ ) is the current extracted from a measurement on the left (right) contact link. The red line is the exact scattering result for the noninteracting system with infinite leads. The other lines are guides to the eye. In agreement with our Kubo calculations the current is enhanced by not too strong repulsive interaction in the low voltage regime. While for large voltages there is a negative differential conductance regime for repulsive interaction.

2000 states per block if not stated otherwise in the legend.

By switching on interaction one sees that the system still displays a conductance for small voltage in agreement with our Kubo calculations. For  $U=0.3$  there is a slight enhancement in the current as compared to the noninteracting case, which is even stronger for  $U=1.0$ . For larger interaction,  $U=5,10$  we do not see a corresponding enhancement, i.e. the resonance width is now reduced. Most strikingly the  $U \geq 1.0$  results show a clear negative differential conductance, i.e. the current gets reduced by increasing the voltage. In order to be sure that this effect is really given by the system and not by truncation errors of the numerics we double checked the results using 3000 states per block for the same system size. In addition we increased the system size to 120 sites to check for finite size effects. For the results (blue symbols, the line is a guide to the eyes) the comparison shows perfect agreement. The negative differential conductance is also very pronounced for strong interaction of  $U=5.0$ , while for  $U=10$  only a very small differential conductance survives. However, for attractive interaction  $U=-1$  the negative differential conductance is absent.

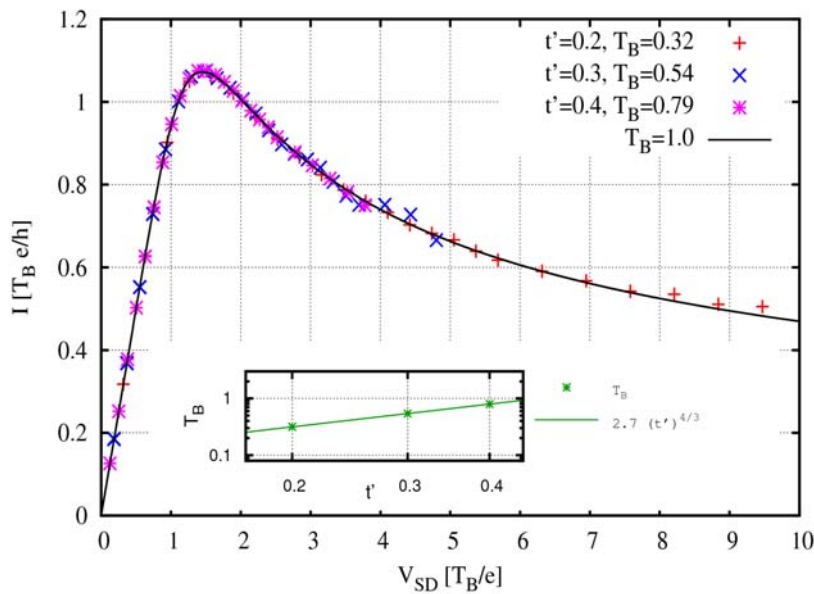


Figure 6: Universal I/V curve at the self dual point  $U=2$ . The numerical data are fitted to the analytical result by a scale  $T_B$ . To ensure a linear conductance of one current and Voltage is rescaled by the same scale. After this rescaling all data collapses on the universal I/V curve. In agreement with the analytical result  $T_B$  scales  $\sim t'^{4/3}$ .

While this effect can currently not be deduced from the scattering state Bethe ansatz of Mehta and Andrei, there exist a special point of interaction, namely the self dual point, where the I/V curve can be obtained from the thermodynamic Bethe ansatz, see [B2.10:11]. Since there the leads are replaced by continuum leads one can only compare results between the field theory and the lattice model up to a regularization scale,  $T_B$ , which depends on the regularization scheme.

In [B2.10:11] we showed that the numerics and the analytical calculation show an excellent agreement, i.e. at the self dual point,  $U=2$ , the data collapses onto a universal curve. We would like to point out that this is the first example of non-equilibrium transport through a strongly correlated nanostructure for which numerical simulations on a lattice and analytical calculations within a field theoretical description show quantitative agreement even far in the nonequilibrium regime. Besides the application to the IRLM we have first results for the I/V curve of the Kondo model in the strong coupling regime.

As a natural extension we looked at the simulation of current-current correlations [B2.10:29-30] concentrating shot noise, the zero frequency limit of

$$S(T, T_0) = \langle \Psi_0 | (\hat{J}(T) - \bar{J}(T)) (\hat{J}(T_0) - \bar{J}(T_0)) | \Psi_0 \rangle$$

$$S = S(\omega \rightarrow 0) = \int_{-\infty}^{\infty} dT e^{i\omega T} S(T)$$

To this end we first have to reach the steady state regime of our simulations at  $T_0$ . We then have to proceed with two independent time evolutions which will provide us with the time resolved noise correlations.

$$|\Psi_L(T)\rangle = e^{-i(\mathcal{H}-E_0)T} |\Psi_0\rangle$$

$$|\Psi_R(T)\rangle = e^{-i(\mathcal{H}-E_0)(T-T_0)} (\hat{J} - \bar{J}) |\Psi_L(T_0)\rangle$$

$$S(T, T_0) = \langle \Psi_L(T) | (\hat{J} - \bar{J}) | \Psi_R(T) \rangle$$

In the following simulations we only used the full td-DMRG [5] without adaptive steps. A major difficulty consists in the strong finite size effects of the zero frequency limit. Since we have to restrict ourselves to finite systems we are actually evaluating the noise correlations at  $\omega \sim 1/M$ , where  $M$  is the number of sites used in the simulation. In [B2.10:30] We have shown that the finite size correction of shot noise for the IRLM are proportional to  $G^2/M$  in the noninteracting case [B2.10:30] and at the self dual point [B2.10:29]. In Fig. 7 we show the results of the simulations of the IRLM at the self-dual point for  $t'=0.3$ . The  $1/M$  extrapolated data show a nice agreement with the analytical result.

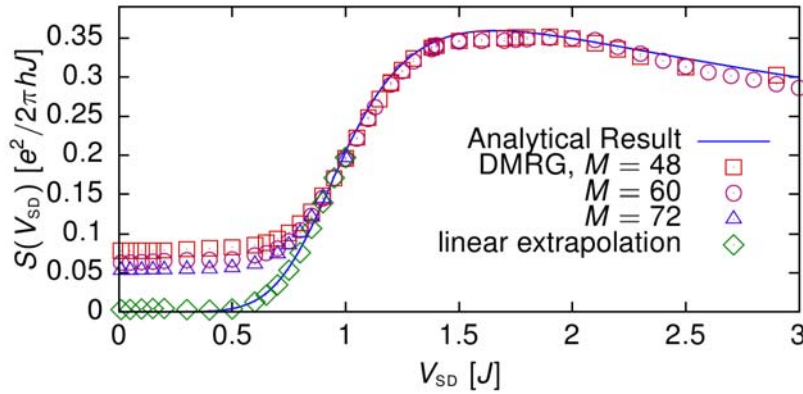


Figure 7: Shot noise of the IRLM at the self dual point. After performing a finite size extrapolation the numerical results agree with the analytical results based on the thermodynamic Bethe ansatz [B2.10:29].

#### 4. Exact Functionals for Density Functional Theory

Density functional theory (DFT) is currently the most applied numerical tool to study the electronic transport through molecules. The Hohenberg-Kohn theorem [7] of density functional theory guarantees that all ground state observables can be obtained from a density functional

evaluated with the ground state density and that the ground state density minimizes the energy functional. In addition, the theorem by Kohn and Sham [8] provides a route to perform DFT calculation practically as they showed that there is a one to one correspondence between an interacting electron system and an auxiliary free noninteracting Fermi system where one replaces the interaction by density potentials, keeping the kinetic term and the local potentials of the interacting system. The theorem states that the ground state densities of the fully interacting system and that of the Kohn-Sham auxiliary system are identical. In addition the Kohn-Sham potentials are unique if the ground state is non-degenerate. While the energy functional is therefore known to exist, the explicit form of the functional for interacting systems is not known and one has to resort to approximations. In DFT calculations one

typically resorts to a local density approximation which may be improved by gradient expansions. One then obtains the eigenfunctions of the Kohn-Sham system and uses those levels to calculate transport properties.

Although this is a widely used approach there are two fundamental problems. The first problem relates to the fact, that „the standard approach“ is based on the Landauer scattering approach. It is true, that the longitudinal current response, as it would be calculated with (a still illusive) exact time dependent density functional theory (TDFT), yields the exact current response via Kubo's formula. Since in addition, also the screened potential can be obtained to calculate the voltage drop, the exact conductance may be found this way. However, there is still an ongoing debate about whether the dynamical approach to the quasistationary nonequilibrium state may indeed be replaced by the much simpler scattering picture [B2.10:5].

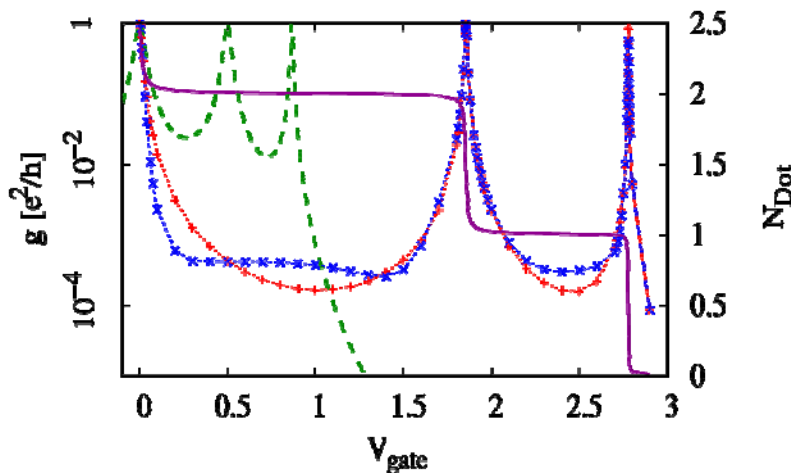


Figure 8: Comparison of the exact conductance (+, dotted line as a guide) and the ground state DFT approximation ( $\square$ , dashed line) for a five site system ( $t'=0.2$ ,  $t_{\text{Dot}}=0.5$ ,  $U=2.0$ ). For comparison the conductance of the noninteracting system ( $U=0$ ) is shown as well (long dashed line). The solid line indicates the particle number of the molecule. The resonances of  $g$  are situated at 0, 1.854, and 2.779 with resonance widths of  $\Gamma=0.026$ , 0.015, and 0.0033.

One of the issues here, relates to the occupation of incoming scattering (Kohn-Sham) states. It is also not clear whether a local approximation to the functional describes interaction effects correctly and it is an open question whether the Kohn-Sham levels are the correct objects to be used for transport calculations. In this project we extended earlier ideas of calculating exact density functionals from DMRG by Gunnarsson and Schönhammer [9,10] to inhomogeneous systems. In short, since we can calculate the local densities from DMRG and due to the uniqueness of the Kohn-Sham potentials, we can start from the exact density and can calculate the corresponding Kohn-Sham potentials by a multidimensional steepest descent method. Details are explained in [B2.10:9]. We then have the exact DFT Kohn-Sham potentials corresponding to our model. The question we now asked is whether by applying the standard procedure of using a Kubo formula for the non-interacting Kohn-Sham levels will actually give the same conductance as the full Kubo calculation within DMRG, compare Bohr and Schmitteckert [B2.10:8]. In this work we coupled a five site nanostructure with a nearest neighbor interaction and a hopping element with a hopping of  $t'=0.2$  to 5 real space lead sites which are then coupled to leads described in energy space, for a detailed description see [B2.10:9].

Even, if indeed a scattering picture based on KS-states of some DFT should be applicable, there is still a question about the implications of approximations to the appropriate exchange-correlation potential. Our recent work suggests, that the self interaction errors in LDA due to the neglect of the so called „derivative discontinuity“ impair the study of Coulomb blockade in DFT based transport calculations [B2.10:1]. Moreover, the missing long-range nature of the potential also implies an overdamping of electronic resonances and therefore an (often

very large) overestimate implicit in theoretical conductance values – as is routinely observed in all (advanced) transport calculations.

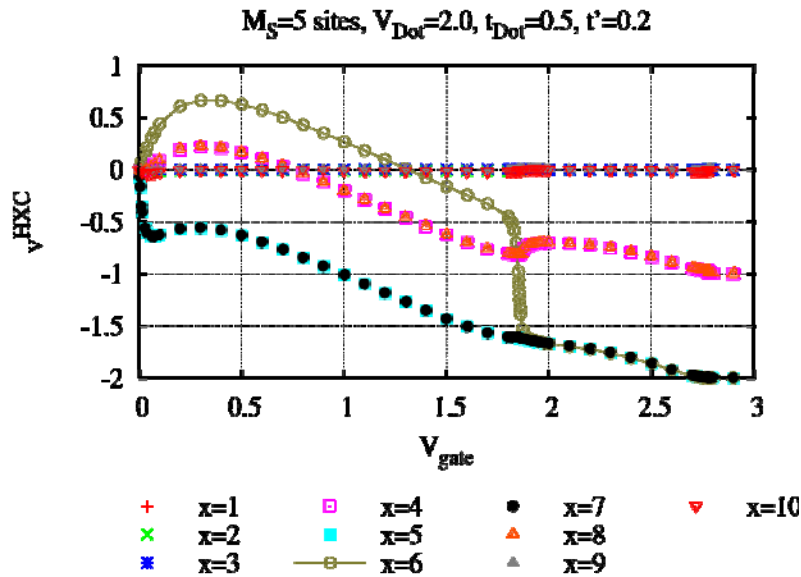


Figure 9: The Kohn-Sham, or Hartree-Exchange-Correlation potential for the nano structure on the attached real space sites vs. applied gate voltage. Sites 4-8 are part of the interacting region. At gate voltages corresponding to resonances in the linear conductance sharp features appear in the Kohn-Sham potentials. Even in the real space lead sites one gets small, albeit nonvanishing Kohn-Sham potentials.

for the real-space sites vs. gate voltage shows that the exact functional contains jumps in the potentials at the resonances as displayed in Fig. 9. There we plot the Kohn-Sham potential vs. the applied gate voltage for the ten real space sites. The increase of the Kohn-Sham potential for the  $x=4,6,8$  sites after resonances is responsible for shifting the resonances to large gate voltages (Coulomb blockade), while the sharp drop at the resonances is responsible for the actual conductance peak.

In conclusion we have demonstrated that the Kohn-Sham level may indeed be sufficient to describe linear transport, at least for well isolated resonances. However one should go beyond local density approximations and one has to include discontinuities in the functionals describing the molecules.

## 5. Light matter interaction in 1D waveguiding structures

In cooperation with Kurt Busch (A1) we simulated the evolution of wave packets consisting of a few photons in a onedimensional wave guiding structure [B2.10:20, B2.10:24] interacting with a two level system. The most striking result of these simulations is that in contrast to the single particle description the few photon wave packet can excite bound states created by the coupling of the two level system to the wave guide. After the scattering event we do not only get a transmitted and reflected wavepacket, but a partial occupation of a bound state can remain, which leads to a partial trapping of the incoming photons at the two level system.

## 6. Other projects

In the projects discussed so far the calculations have been restricted to model Hamiltonians. In a first step to simulate quantum chemistry type models described by

In Fig. 8 we compare the linear conductance obtained from the DMRG calculation with the one obtained from the Kohn-Sham levels. The results show a surprising agreement close to the resonance capturing the shift in position (Coulomb blockade) and the change in the resonance width. Only in the tails of the resonances there is a significant deviation. However, a careful analysis of the data reveals that the exact Kohn-Sham functional is non-local. For instance it is not single valued if the local potentials are plotted against the local densities. In addition, a plot of the Kohn-Sham potential

$$\mathcal{H} = \sum_{p,q,l,m} V_{p,q,l,m} \hat{c}_p^+ \hat{c}_q^+ \hat{c}_l \hat{c}_m$$

we implemented the above Hamiltonian with  $V_{p,q,l,m}$  given by the problem of a two dimensional electron gas in a strong magnetic field where the angular degrees of freedom are integrated out. For this one has to carefully implement the minus signs appearing from the fermionic nature of the electrons. A comparison with an exact diagonalization programme of Xin Wan showed that we successfully implemented this Hamiltonian, see Hu, Wan and Schmitteckert [B2.10:15]. In cooperation with Karin Fink we are currently developing an interface to the quantum chemistry codes used at the INT.

In [B2.10:10] we discuss the sign of the persistent current of  $N$  electrons in one dimensional rings. Using a topology argument, we establish lower bounds for the free energy in the presence of arbitrary electron-electron interactions and external potentials. Those bounds are the counterparts of upper bounds derived by Leggett. Rings with odd (even) numbers of polarized electrons are always diamagnetic (paramagnetic). We show that unpolarized electrons with  $N$  being a multiple of four exhibit either paramagnetic behavior or a super conductor like current-phase relation.

In [B2.10:4] we showed that in fermionic atoms in two different hyperfine states confined in optical lattices show strong commensurability effects due to the interplay between the atomic density wave ordering and the lattice potential. We show that spatially separated regions of commensurable and incommensurable phases can coexist. The commensurability between the harmonic trap and the lattice sites can be used to control the amplitude of the atomic density waves in the central region of the trap. Recently we extended that work to study dynamics within strongly correlated cold atom gases [B2.10:21].

## 7. Current projects

### 7.1. Full Counting statistics

Motivated by the success of calculating current and shot noise from time dependent simulations we have implemented the the simulation of the cumulant generating function (CGF)  $Z$  [12,13]

$$\mathcal{H}_\chi = \mathcal{H} + \left( t_1 e^{i\chi/2} - t \right) \hat{c}_{n_1}^+ \hat{c}_{n_1-1} + \left( t_1 e^{-i\chi/2} - t \right) \hat{c}_{n_1-1}^+ \hat{c}_{n_1}$$

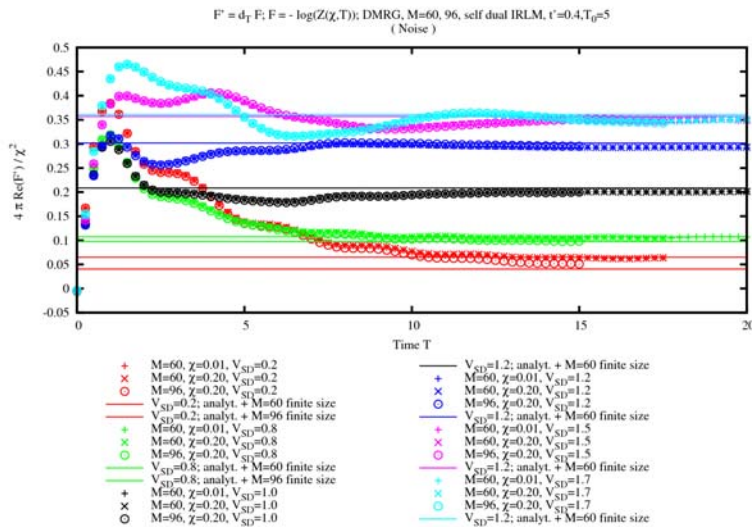


Figure 10: Extraction of shot noise from time dependent simulations for the IRLM at the self dual point by dividing the time derivative of the CGF by  $\chi^2$ . The results are in agreement with the results obtained from a direct simulation of the current current simulations and the analytical result, provide finite size corrections are taken into account.

where similar to the shot noise correlations we first evolve the system after the voltage quench to the quasi-stationary regime. Then we switch on a counting field  $\chi$  at time  $T_0$  and perform a forward evolution in time  $T$  with a positive counting field  $\chi$  and a backward evolution with  $-\chi$ .

$$|\Psi_\chi(T)\rangle = e^{-i(\mathcal{H}_\chi - E_0)(T - T_0)} |\Psi(T_0)\rangle$$

The CGF  $Z(\chi, T)$  has the interesting property that the first derivative with respect to the counting field is proportional to the current, the second derivative is

proportional to shot noise and higher derivatives provide higher cumulants. The extraction of shot noise from  $Z(\chi, T)$  for the IRLM at the self dual point is displayed in Fig. 10. Currently we are performing simulations for large counting fields in order to obtain the complete FCS.

## 7.2 Adiabatic state evolution

As a complementary tool to the time evolution we developed a new state evolution scheme

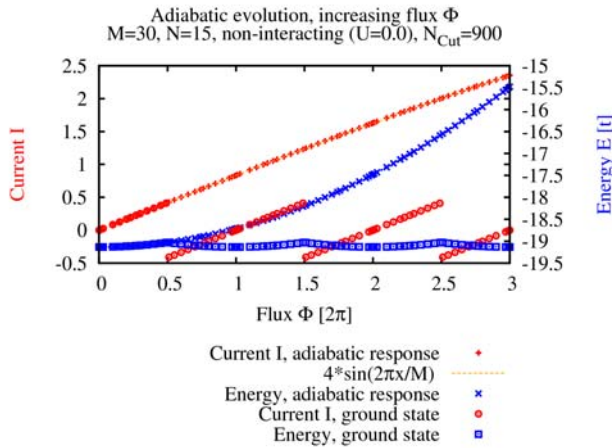


Figure 11: Current and energy of a onedimensional ring of spinless fermions obtained by an adiabatic tracking of the response of a flux threatening the ring vs. the ground state.

where we track the adiabatic response of a state to an external perturbation. As a first example we looked at the response of a model of spinless fermions in a onedimensional ring, where we follow the response to flux threatening the ring. In Figure 11 we compare the energy and the current of a 30 site systems of noninteracting fermions on a ring obtained from our adiabatic state tracking within DMRG flux vs. a standard ground state calculation. While the ground state calculation is periodic in the flux, we can track the adiabatic response into the metastable region. By switching on interactions adiabatically we have now access to current carrying states which are eigenstates of the system. We would like to note that the concept of switching on perturbations/interaction

adiabatically is at the heart of analytical tools based on scattering theory.

## 7.3 Reflectionless impurities as boundary condition

One of the major difficulties in simulating correlated quantum systems lies in the restriction to finite systems. In his seminal work on the numerical renormalization group Wilson showed that for impurity problems one can model large leads by a rather small tight binding chain provided the hopping elements are exponentially decreasing towards the boundary. This concept is extended within the DMRG as *smooth* or *damped* boundary conditions, where the exponentially decreasing region is put at the end of an unperturbed hopping chain. While this approach turned out to be successful for static problems it has the problem that within the damped region every link provides a perturbation that creates backscattering, for details see the discussion of the NRG tsunami in [B2.10:25]. It is therefore problematic to study systems close to resonance as the leads themselves already create reflections. In order to overcome this problem we replaced the exponentially decreasing hopping elements by integrable impurities which have a similar property of enhancing the density of states close to the Fermi surface. However, due to the construction of the impurities via the Quantum Inverse Scattering method, the impurities are reflectionless. Note that this kind of impurities exists even in the presence of nearest neighbour interaction and are derived in [11]. In Fig. 12 we show that this property of the algebraic Bethe ansatz persists in time dependent simulations, where similar to the simulation of the spin-charge separation we send a wave packet through a region including the integrable impurities.

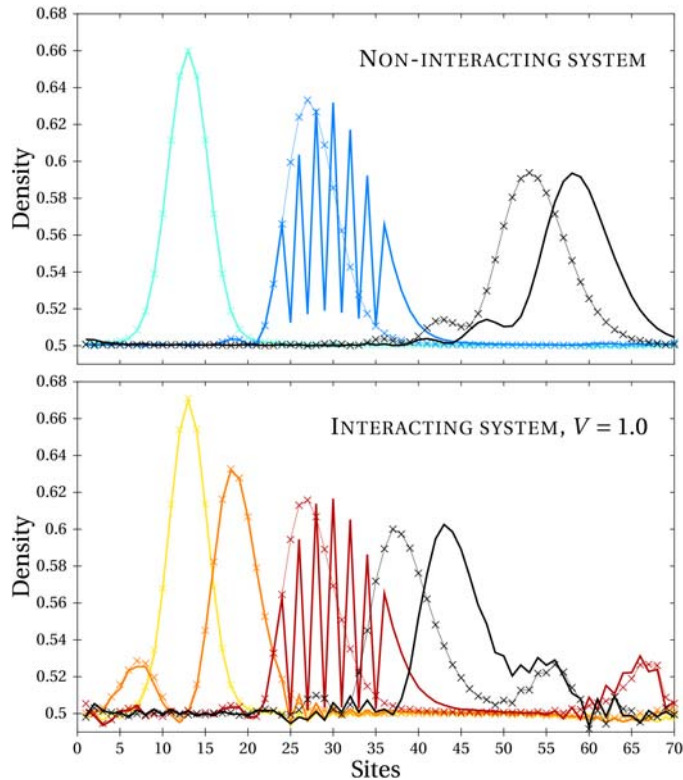


Figure 12: Evolution of a wave packet in a 1D system of spinless fermions in the presence of six integrable impurities of strength  $nu=6t$  in the middle of the system. The line with symbols correspond to a reference system without impurities. The upper graph corresponds to a noninteracting system, the lower to a system with a nearest neighbour interaction of  $U=1t$ , with  $t$  the nearest-neighbour hopping amplitude.

Despite the strong impurity strength, the impurities do not create a reflected wave. The additional peak appearing for finite interaction comes from the splitting of the inserted fermion into left and right moving excitation of the underlying Luttinger liquid. We have applied this kind of impurities as a boundary system within the embedding method, compare [B2.10:10], and have preliminary results showing that the integrable impurities allow to access narrow conductance peaks, where calculations based on damped boundary conditions are dominated by the reflection of boundary scatterer instead of the nanostructure of interest.

## 7.4 Driven systems

We have extended our simulations by the possibility to switch between different Hamiltonians which are governing the time evolution. Currently we are testing our implementation by studying the parametric resonance of a Luttinger liquid in response to a periodic perturbation.

## 7.5 Chebychev expansions within DMRG

We have developed the evaluation of matrix exponentials and resolvents within the framework of Chebychev expansions. Instead of evaluating a matrix exponential of a resolvent corresponding to a Greens function directly we have implemented a recursive evaluation of the orthogonal polynomial, typically using Chebychev polynomials, of an Hamiltonian. Based on the moments of the orthogonal polynomials we are able to reconstruct the desired function. As a first result we have been able to calculate the spectral function of the interacting resonant level model for various interaction strength using the expansion into Chebychev polynomials.

## 8. Transport through quantum wires: Junctions of Luttinger liquids

A number of methods are available to describe electron transport through quantum dots coupled to non-interacting leads. The justification for neglecting the interaction in the leads is that in a three-dimensional metal the Coulomb interaction is screened and in addition, Fermi liquid theory holds, allowing a description in terms of non-interacting quasi-particles. By contrast, in truly one-dimensional wires the effect of the interaction is to destroy the Fermi

liquid state. Conventionally 1d electron systems are described in terms of their bosonic excitations, in a procedure called bosonization. However, in situations where the wire is attached to (massive) leads, this is not a good starting point. The reason is that electrons entering the wire would have to be converted into bosonic excitations, which at the end of the wire must combine to give back an electron. In early work [14] an infinite wire has been considered. It was found that in the (usual) case of repulsive interaction a barrier has the effect of blocking the transport completely, in the limit  $T \rightarrow 0$ . In these works the conductance of the ideal Luttinger liquid (no barrier) has been calculated to be given by the Luttinger parameter  $K$  (in units of the quantum of conductance  $e^2/h$ ), whereas it should be 1 (two-terminal conductance). The correct interpretation of this result, in our view, is that in these works the screening of the applied field was not taken into account [15].

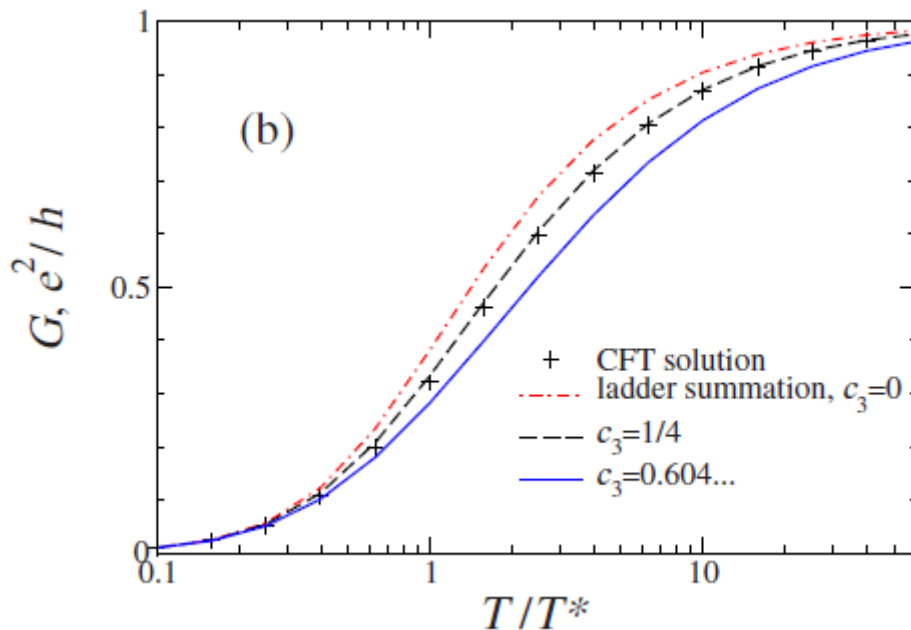


Figure 13: Linear conductance of a Luttinger liquid wire with barrier at the special interaction strength  $K=1/2$  versus temperature. The “ladder summation” result (red curve) becomes exact at low  $T$ , but deviates from the exact conformal field theory result (multiplied by a factor 2) at intermediate  $T$ . The result of including higher order terms with coefficient  $c_3$  is also shown.

Conceptually it is much simpler to calculate the conductance in fermionic language. This has been done in [16] in a renormalization group treatment for a model of spinless fermions in lowest order in the interaction. We have extended this work to all orders in the interaction [B2.10:25,26], i.e. we have calculated the RG beta-function to all orders by summing an infinite class of diagrams. This is possible in the current algebra representation, which allows to organize the perturbation theory in a particularly efficient way [B2.10:26]. As a result we find an analytic expression for the conductance, which completely agrees with the scaling behavior at low temperature found by many other methods, but in addition has the correct high temperature behaviour (Fig. 13). At intermediate temperatures we have found corrections to our ladder approximation, which shed a new light on the question of universality of the beta-function. Work is in progress to extend our treatment to nonequilibrium. Also, the effect of spin will be incorporated in future work.

More recently we have extended this approach to Y-junctions, describing the tunnelling from a tip into a quantum wire. We find that the statement one often finds in the literature, that for repulsive interaction the system scales to a fixed point with the tip detached and the wire

being unaffected by the tip (ideal conductor), is not correct. We show that this result is not valid in any realistic situation: rather, the three wires will be completely detached in the limit of zero temperature [B2.10:27]. Another interesting observation is that the conductance as a function of temperature may generically show nonmonotonical behaviour. So far these results were derived for weak interaction. An extension to strong interaction, following the approach used in the two-terminal case, is possible (work in progress).

The Luttinger liquid description is restricted to low energy excitations for which the fermion energy spectrum may be linearized. A first extension of this treatment has been formulated in [B2.10:28].

## References

- [1] E. A. Jagla, K. Hallberg and C. A. Balseiro, *Phys. Rev. B* **47**, 5849 (1993).
- [2] C. Kollath, U. Schollwöck and W. Zwerger, *Phys. Rev. Lett.* **95**, 176401 (2005).
- [3] S. R. White and A. E. Feiguin, *Phys. Rev. Lett.* **93**, 076401 (2004).
- [4] A. J. Daley, C. Kollath, U. Schollwöck and G. Vidal, *J. Stat. Mech.: Theor. Exp.* P04005 (2004).
- [5] Peter Schmitteckert: *Nonequilibrium electron transport using the density matrix renormalization group*, *Phys. Rev. B* **70**, 121302 (2004).
- [6] P. Mehta and N. Andrei, *Phys. Rev. Lett.* **96**, 216802 (2006).
- [7] P. Hohenberg and W. Kohn, *Phys. Rev.* **136**, B864 (1964).
- [8] W. Kohn and L. J. Sham, *Phys. Rev.* **140**, A1133 (1965).
- [9] O. Gunnarsson and K. Schönhammer, *Phys. Rev. Lett.* **56**, 1968 (1986).
- [10] K. Schönhammer, O. Gunnarsson, and R. M. Noack, *Phys. Rev. B* **52**, 2504 (1995).
- [11] P. Schmitteckert, P. Schwab, and U. Eckern, *Quantum Coherence in an Exactly Solvable One-dimensional Model with Defects*, *Europhys. Lett.* **30**, 543 (1995).
- [12] L.S. Levitov and G.B. Lesovik, *JETP Lett.* **58**, 230 (1993).
- [13] K. Schönhammer, *Phys. Rev. B* **75**, 205329 (2007).
- [14] C. Kane and M.P.A. Fisher, *Phys. Rev. Lett.* **68**, 1220 (1992).
- [15] Y. Oreg and A.M. Finkel'stein, *Phys. Rev. B* **54**, 14265 (1996).
- [16] D. Yue, L. I. Glazman and K. A. Matveev, *Phys. Rev. B* **49**, 1966 (1994).